Title

Energy-chirp compensation of laser-driven ion beams enabled by structured targets

Authors

Gong, Z
Bulanov, SS
Toncian, T
et al.

Publication Date

2018-07-19

Peer reviewed

Laser ion-shotgun acceleration

A. V. Arefiev,[1] Z. Gong,[2] T. Toncian,[3] and S. S. Bulanov[4]

[1] *University of California at San Diego, La Jolla, CA 92093, USA*
[2] *Center for High Energy Density Science, The University of Texas at Austin, Austin, TX 78712, USA*
[3] *Institute for Radiation Physics, Helmholtz-Zentrum Dresden-Rossendorf e.V., 01328 Dresden, Germany*
[4] *Lawrence Berkeley National Laboratory, Berkeley, California 94720, USA*

Relativistic transparency induced by an ultra-intense laser (5×10^{22} W/cm^2) offers an attractive method for generating extreme electric (50 TV/m) and magnetic (0.5 MT) fields by enabling laser pulse propagation through a very dense and otherwise opaque material. A slowly evolving structure that effectively accelerates ions is generated by employing a target (~ 10 μm thick) with a pre-filled channel that guides the laser pulse. As the pulse exits the channel driving a strong electron current, strong accelerating longitudinal and focusing transverse electric fields emerge at the rear side of the target. Three-dimensional kinetic simulations predict a low-diverging dense mono-energetic proton bunch with energies of 200-300 MeV. The charge in an opening angle of 10° is tens of nC. This scheme potentially allows high repetition rate operation and relaxes laser contrast requirements.

Laser-driven ion acceleration [1–4] is one of the main applications for the current and future high-power laser systems around the world [5–7]. The interest in developing high energy laser-driven ion beams is not surprising, as such beams are critical for a variety of cross-disciplinary applications [8–12]. They are also essential for fundamental studies of laser-matter interactions and for the development of advanced concepts of particle acceleration [1–3].

Typically, the ion acceleration is achieved by laser irradiation of thin solid-density foils [13–18]. The acceleration regimes vary depending on the laser intensity and the target surface density [19], but all of them are sensitive to prepulse characteristics of the driving laser pulse. The impact of the prepulse is usually detrimental. Ultra-thin targets can even lose their integrity because of the prepulse prior to the arrival of the main pulse [20].

In an attempt to mitigate the role of the prepulse, acceleration mechanisms involving near-critical density targets have been developed (e.g., magnetic vortex acceleration [21–25], shock wave acceleration [26], hole-boring radiation pressure acceleration [27–29]). In this case, the ion acceleration is determined primarily by the laser interaction with the bulk of the thick target, reducing the importance of the prepulse that affects the surface.

Experimental realization of the described mechanisms [23, 25, 26, 30] is evidently a serious challenge, since the maximum proton energies have remained below 100 MeV [31, 33, 34] despite a significant increase of the peak laser intensities over the past decade. In the case of thin foils, the laser prepulse is the culprit, whereas, in the case of near-critical targets, the difficulty is manufacturing an optimal target configuration. Reaching high proton energies is not sufficient to meet the requirements of the proposed applications for the laser-driven proton beams. A typical exponentially decaying spectrum has only a handful of protons with energies close to the maximum energy. In contrast to that, most applications require a spectrum with mono-energetic features in the energy range of interest and a relatively low angular divergence.

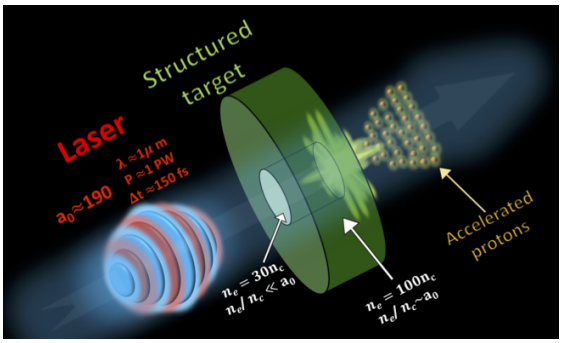

FIG. 1: Schematic setup [not to scale] for the laser ion-shotgun acceleration mechanism that generates dense and collimated mono-energetic proton beams.

In this Letter, we report on a novel laser-driven ion acceleration mechanism, termed the laser ion-shotgun acceleration. It involves a structured target and the effect of relativistically induced transparency to enable a volumetric laser-matter interaction at solid densities that leads to generation of a mono-energetic proton beam whose energy reaches several hundred MeV. Our fully-kinetic relativistic three-dimensional particle-in-cell (3D PIC) simulations predict an unprecedented beam charge, tens of nC, and relatively low angular divergence, below 10°, even for a 1 PW laser pulse with a peak intensity of 5×10^{22} W/cm^2.

The structured target, schematically shown in Fig. 1, is a solid-density slab with a channel pre-filled with a dense solid material that becomes transparent only when irradiated by a high-intensity laser pulse. The laser pulse is tightly focused at the entry of the channel to ensure its efficient coupling to the channel and its subsequent guiding due to the relativistically transparency. In our study, we use a pulse with a wavelength of $\lambda = 1$ μm and a peak intensity of $I = 5 \times 10^{22}$ W/cm^2, so that the normalized amplitude, defined as $a_0 \approx 0.85 \times 10^{-9} \lambda[\mu\text{m}] \sqrt{I[\text{W/cm}^2]}$,

is roughly $a_0 \approx 190$. A laser of this intensity quickly ionizes the irradiated material, turning it into a plasma. The plasma is transparent due to the relativistic electron motion in the laser pulse if the electron density satisfies the condition $n_e \ll a_0 n_{cr}$, where $n_{cr} \equiv m_e\omega^2/4\pi n_e e^2$ is the classical critical density that determines plasma transparency for $a_0 \leq 1$, ω is the carrier frequency of the pulse, m_e and e are the electron mass and charge. The density inside the channel of the structured target is set at $n_e = 30n_{cr}$, whereas the density in the bulk is set at $n_e = 100n_{cr}$, which enables stable optical guiding of the irradiating laser pulse through the overdense plasma ($n_e \gg n_{cr}$). Such a target can be manufactured using the already existing technology and variable density foams [35].

The target structure plays an important role. If the target is uniform with $n_e = 30n_{cr}$, then the head of the focused laser beam expels electrons radially outwards and produces an ion channel fully devoid of electrons. In our case, the laser electric field successfully counteracts the expulsion by ripping electrons out of the channel walls and injecting them back into the laser pulse, as shown in Fig. 2a. The injected electrons, whose density significantly exceeds n_{cr}, are accelerated forward by the laser, producing a strong longitudinal current and generating an extreme azimuthal magnetic field. As shown in Fig. 2d, the amplitude of this slowly evolving field reaches 0.5 MT, which is an appreciable fraction of the laser magnetic field [36, 37]. The field is contained inside the channel, since there is also a current flowing along the walls of the channel, thus producing a structure similar to a co-axial wire – a co-axial plasma channel.

The magnetic field is effectively leveraged for ion acceleration by employing a finite-length target, such that the pulse is able to exit the channel without being depleted and generate an accelerating field structure. The key features are shown in Fig. 2, where the snapshots are from a 3D PIC simulation for a 15 μm long target. In this simulation, the longitudinal and transverse resolutions are 20 and 15 cells per μm. The target is fully ionized, with the channel material being hydrogen and the bulk material being carbon. The electrons and carbon ions are represented by 10 macro-particles per cell. We use 50 macro-particles per cell to represent the protons in the channel in order to obtain a well-resolved spectrum. The channel radius in this case is $R_{ch} = 1.8$ μm. The laser focal plane is at $x = 0$ μm, with a $w_0 = 2.2$ μm focal spot. The duration of the considered Gaussian pulse is 150 fs. The other parameters are the same as before.

Energetic electrons accelerated by the laser in the channel overtake the pulse and emerge at the rear side of the target before the pulse. They set up a sheath electric field normal to the surface that starts to accelerate ions and protons. However, this mechanism can only generate a strongly divergent beam with an exponentially decaying spectrum (see Figs. 3a and 3c).

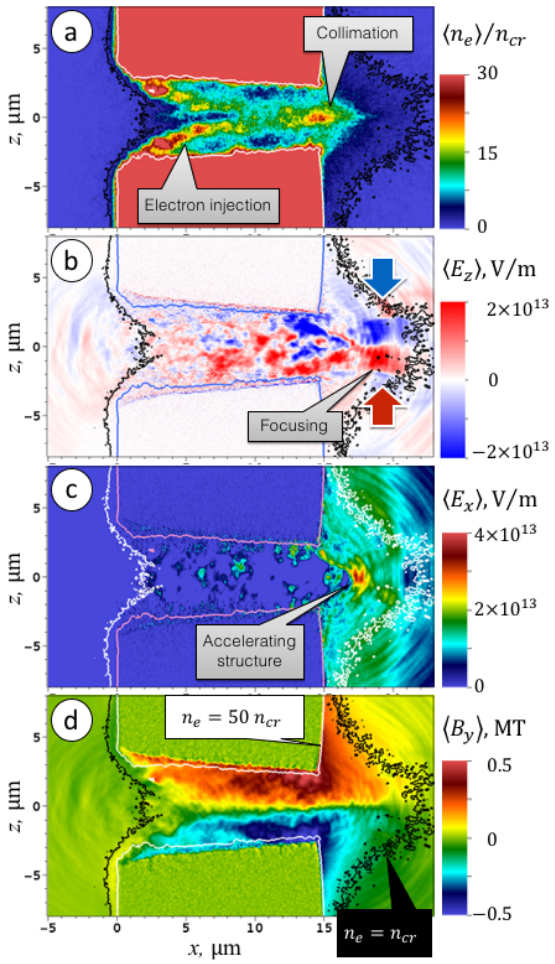

FIG. 2: Accelerating structure that produces a monoenergetic proton beam in 3D PIC simulations. All quantities are averaged over one laser period and plotted in the (x, z)-plane at $y = 0$ μm. A similar structure exists in the (x, y)-plane.

As the laser reaches the rear side and exists the target, the accelerating field structure changes in a dramatic way (see Figs. 2b and 2c): the longitudinal field $\langle E_x \rangle$ develops a moving peak that is accompanied by a strong focusing field $\langle E_z \rangle$. The brackets indicate laser-cycle averaging. The observed structure is generated due to the pinching of the electron current driven by the laser pulse. The current is relativistic, so it quickly catches up with the expanding proton cloud and begins to modify the proton spectrum. The strong electric field of the current attracts the protons towards the laser axis. This leads to a well-collimated quasi-monoenergetic proton beam shown in Figs. 3d. Prior to the arrival of the pinched current, the proton distribution in the transverse momentum plane (p_y, p_z) has a ring-type structure that is rather broad, with a characteristic opening angle of 20°. After the interaction with the transverse fields of the electron current, a strong pinching of the proton distribution takes

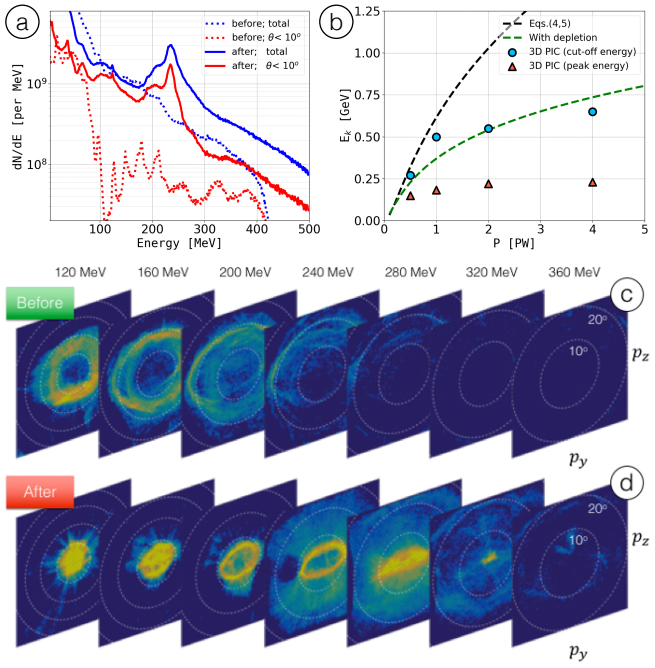

FIG. 3: The proton spectra (a) and angular distribution (c,d) *before* and *after* the ion-shotgun acceleration. Estimates for proton kinetic energies E_k together with 3D PIC results are shown in (b) for different values of average laser power P.

place. The analysis of the spectra in Fig. 3a reinforces this conclusion. Prior to the interaction, the number of protons in a 10° opening angle is negligible. However, after the interaction, the 10° spectrum almost matches the total spectrum in the 100 - 300 MeV energy range, indicating that almost all of the protons are concentrated in a 10° cone. Evidently, the channel is akin to a barrel of a shotgun that builds up an expulsion force and propels a bullet, which, in our case, is the collimated proton beam. That is why we refer to the mechanism as the laser ion-shotgun acceleration.

In order to determine how the energy of the peak scales with laser power P, we have performed a parameter scan where the laser peak intensity was fixed, while the channel radius and the focal spot were increased proportionally to keep their ratio at $w_0/R_{ch} \approx 1.2$. The scan with $w_0 \approx 1.1$, 1.54, 2.2, and 2.5 μm corresponds to an average power of $P \approx 0.5$, 1, 2, and 4 PW. The results shown in Fig. 3b indicate that both the cut-off energy and the energy of the monoenergetic peak saturate above 2 PW. It should be mentioned that the peak is no longer pronounced at 4 PW, possibly due to laser filamentation.

In order to elucidate the obtained scaling, we provide analytical estimates for proton energies that are based on the key features observed in our 3D simulations. We assume that the laser propagation is similar to propagation of an electromagnetic wave through a cylindrical waveguide. Following Refs. [38, 39], we compare the amplitude of the wave in the waveguide, a_{ch}, with the amplitude of the same wave in vacuum to find that

$$a_{ch} = \pi^{-1} \left(\lambda/\pi R_{ch}\right) \left(2P/KP_c\right)^{1/2}, \qquad (1)$$

where $K = 0.074$ is the factor coming from the integration of laser intensity distribution over space and time; $P_c = 2m_e^2c^5/e^2 \approx 17$ GW; R_{ch} is the channel radius; $P = W/\tau$ is the laser power, W is the laser energy, and τ is the laser pulse duration. The group velocity of the wave in the channel is $v_g/c = 1 - \left(\kappa\lambda/2\pi\right)^2$, where κ is the solution of the equation, $J_1'(\kappa R_{ch}) = 0$, which comes from the wave equation in the waveguide. Here J_1 is the Bessel function and $\kappa R_{ch} = 1.84$.

Equation (1) is only applicable if the laser beam is confined by the channel walls. If the plasma density in the channel is high enough to contain the laser pulse without the help of high density walls, i.e., $R_{sc} < R_{ch}$, a different set of equations, the ones from Refs. [38, 39] should be used, where $R_{sc} = \lambda/\pi \left(2/K\right)^{1/6} \left(n_{cr}^2 P/n_e^2 P_c\right)^{1/6}$, $a_{sc} = \left(2/K\right)^{1/3} \left(n_e P/n_{cr} P_c\right)^{1/3}$. Here the subscript (sc) stands for the self-created and indicates that the laser creates the channel in the electron density by evacuating the electrons in the transverse direction. The channel radius is then determined from balancing the energy gain of electrons in the laser field and the energy gain in the field of an ion column.

Our regime of interest implies that $R_{sc} \geq R_{ch}$. An intense laser pulse propagating inside the channel of radius R_{ch} drives a current through this channel, injecting electrons from the walls and from the channel entry, as it was shown in simulation results above. The electron density of this current, n_e^j, is estimated from the condition $R_{sc}(n_e^j) = R_{ch}$, which yields

$$n_e^j/n_{cr} = \left(2/K\right)^{1/2} \left(\lambda/\pi R_{ch}\right)^3 \left(P/P_c\right)^{1/2}. \qquad (2)$$

The current sustains the strong magnetic field inside the channel: $eB/m_e\omega c = \left(2/K\right)^{1/2} \left(r\lambda^2/\pi^3 R_{ch}^3\right) \left(P/P_c\right)^{1/2}$ for $r < R_{ch}$. The maximum value of this field at $r = R_{ch}$ is $B_{max} = E_0(2/K)^{1/2}\pi^{-3}\lambda/R_{ch} \approx 0.16 E_0\lambda/R_{ch}$, where E_0 is the vacuum amplitude of the laser field for the focal spot equal to R_{ch}. If such a field generates an electric field of comparable amplitude at the exit from the channel [38, 39], then the electric field would not be able to accelerate ions to high energies. However, as the interaction evolves, the laser leaves the channel and the electron current left in its wake begins to pinch towards the channel axis. This leads to a significant intensification of the field:

$$\frac{eB_{r=R_b}}{m_e\omega c} = \frac{2\pi^3}{(\kappa R_{ch})^2} \frac{n_e^j}{n_{cr}} \left(\frac{R_{ch}}{\lambda}\right)^3, \qquad (3)$$

with the characteristic size of the pinched current $R_b = R_{ch}/\gamma_e$, here γ_e is the average gamma-factor of the electrons in the current. We assume that it is equal to

the gamma-factor of the laser, $\gamma_e = \left(\sqrt{2}/1.84\right)\pi R_{ch}/\lambda$, which is determined by its group velocity [38, 39].

This pinched current should be localized, since the laser pulse is no longer injecting the electrons from the walls to sustain the current. The characteristic longitudinal extent should be of the order of the relativistic plasma wavelength. As this localized current moves out of the channel at relativistic velocity ($\gamma_e \gg 1$), the field associated with it begins to accelerate the protons. However, due to the fact that these fields move with the current, the overall acceleration efficiency depends on the actual overlap between the protons and the electric current. The maximum energy gain in such moving field can be estimated as follows. We assume that initially the protons are at rest, then the acceleration is in effect while $ct - x < R_{ch}$, where $x = x(t)$ is the proton coordinate. The accelerating field is of the order of the magnetic field, generated by the current, $E \approx B_{r=R_b}$. Then we solve the equation of motion $dp_i/d(\omega t) = eE/m_i\omega c$, which yields

$$\left[-1 + 3p_i + p_i^3 + (1+p_i^2)\sqrt{1+p_i^2}\right] = 3eER_{ch}, \quad (4)$$

where m_i the ion mass, p_i is the momentum normalized to $m_i c$ and

$$\frac{eER_{ch}}{m_e\omega c} = \frac{2}{(1.84)^2}\left(\frac{2P}{KP_c}\right)^{1/2} R_{ch}. \quad (5)$$

According to the solution of Eq. (4) the ion kinetic energy, $E_k/m_ic^2 \equiv \sqrt{1+p_i^2} - 1$, scales as $E_k \propto P$ for $P \ll 1$ PW and $E_k \sim P^{3/8}$ for $P \gg 1$ PW. Moreover in the interval 0.5 PW $< P <$ 1.8 PW the ion kinetic energy scales as $E_k \propto P$ with a 5% accuracy. In order to obtain this scaling we assumed that the channel radius scales as $R_{ch} \propto \sqrt{P}$. For $P = 1$ PW and $R_{ch} \approx 1.3$ μm, we obtain the maximum proton energy of about 0.7 GeV, for $P = 2$ PW and $R_{ch} \approx 1.8$ μm, it is 1.2 GeV.

We note that the comparison of the PIC simulation results and analytical estimates shows a significantly smaller maximum proton energy in the former case. It is due to the fact that in the analytical estimate the laser pulse depletion, as it propagates in the channel, as well as the efficiency of the laser pulse coupling to the channel are neglected. One can then interpret Eqs. (4) and (5) as upper estimates for the maximum proton energy. The effectiveness of coupling can depend on a number of factors, connected with the laser pulse energy transformation into the energy of electrons and the formation of the current. First, as the channel radius increases with laser power it takes more time for the electrons from the walls of the channel to reach the axis and be captured by the laser. Second, the laser f-number determines at what angle the laser pulse interacts with the channel entry, from where a significant number of electrons is injected into the laser pulse (see Fig. 2a). Both of these effects should lead to an additional factor on the right-hand side of Eq. (4), with the factor being inversely proportional to the radius of the channel, $3eER_{ch} \to 3eE$. This simple estimate of the coupling effect together with depletion taken into account agrees better with the PIC simulation results (see Fig. 3b). Since in our PIC simulations we fixed the peak vacuum intensity of the laser and varied laser power, f-number, and radius of the channel accordingly, the dependence of this mechanism efficiency on these parameters separately was not studied. We plan to address this in a followup publication.

In conclusion, we presented a novel mechanism of laser ion acceleration from a structured target, which potentially allows high repetition rate operation that is soon to become the state of the art in the field [41] and relaxes the requirements on the laser contrast. We chose a prefilled channel target, which is a solid density slab with the thickness of 15 μm and a channel of a couple of μm radius drilled in this slab and filled with a relativistically near critical density hydrogen. Such interaction setup ensures stable propagation of an intense laser pulse in the channel, as well as a generation of strong electromagnetic fields due to strong currents driven by the laser inside the channel. These fields are able to accelerated protons from the channel to high energies. The analytical estimates reveal the scaling of maximum kinetic ion energy of $E_k \propto P$ for PW-class laser pulses, which changes into a less favorable one $E_k \propto P^{3/8}$, $P \gg 1$ PW, as the ions become ultra-relativistic. Moreover, the evolution of the electron current inside the channel in the course of interaction produces a highly localized field structure that positively impacts accelerated protons. As this field moves with the pinched electron current through an expanding proton cloud at the back of the target, it focuses protons into a well defined collimated quasi-monoenergetic beam. The 3D PIC simulations show the production of accelerated protons with the maximum energy of about 600 MeV, the quasi-monoenergetic peak at 280 MeV by 2 PW 150 fs laser pulse. The number of protons in the energy interval 200-300 MeV is about 8×10^{10} particles, which is a charge of 12 nC. Such beam parameters may be of interest for various applications that require high energy, high repetition rate, high charge, quasi-monoenergetic proton sources.

The research was supported by NSF (Cont. No. 1632777) and AFOSR (Cont. No. FA9550-17-1-0382). SSB acknowledges support by Laboratory Directed Research and Development (LDRD) funding from Lawrence Berkeley National Laboratory provided by the Director, and the U.S. Department of Energy Office of Science Offices of High Energy Physics and Fusion Energy Sciences, under Contract No. DE-AC02-05CH11231. Simulations were performed using EPOCH [40], developed under UK EPSRC grants EP/G054940, EP/G055165 and EP/G056803. HPC resources were provided by TACC.

[1] G. Mourou, T. Tajima, and S. V. Bulanov, Rev. Mod. Phys. **78**, 309 (2006).

[2] H. Daido, M. Nishiuchi, and A. S. Pirozhkov, Reports on Progress in Physics **75**, 056401 (2012).

[3] A. Macchi, M. Borghesi, and M. Passoni, Rev. Mod. Phys. **85**, 751 (2013).

[4] S. V. Bulanov, Ja. J. Wilkens, T. Zh. Esirkepov, G. Korn, G. Kraft, S. Kraft, M. Molls, and V. S. Khoroshkov, Phys. Usp. **57**, 1149 (2014).

[5] M. Dunne, Nature Phys. **2**, 2 (2006); *ELI-Extreme Light Infrastructure Science and Technology with Ultra-Intense Lasers WHITEBOOK*, edited by G. A. Mourou, G. Korn, W. Sandner, and J. L. Collier (THOSS Media GmbH, Berlin, 2011).

[6] C. Danson, D. Hillier, N. Hopps, and D. Neely, High Power Laser Science and Engineering **3**, e3 (2015).

[7] K. Nakamura, H. S. Mao, A. J. Gonsalves, H. Vincenti, D. E. Mittelberger, J. Daniels, A. Magana, C. Toth, and W. P. Leemans, IEEE Journal of Quantum Electronics **53**, 1 (2017).

[8] K. Krushelnick, E. L. Clark, R. Allott, F. N. Beg, C. N. Danson, A. Machacek, V. Malka, Z. Najmudin, D. Neely, P. A. Norreys, M. R. Salvati, M. I. K. Santala, M. Tatarakis, I. Watts, M. Zepf, and A. E. Dangor, IEEE Trans. Plasma Sci. **28**, 1110-1155 (2000).

[9] M. Borghesi, J. Fuchs, S. V. Bulanov, A. J. Mackinnon, P. K. Patel, and M. Roth, Fusion Sci. Technol. **49**, 412 (2006).

[10] M. Barberio, M. Sciscio, S. Vallieres, F. Cardelli, S. N. Chen, G. Famulari, T. Gangolf, G. Revet, A. Schiavi, M. Senzacqua, and P. Antici, Nature Comm. **9**, 372 (2018).

[11] R. L. Pease, A. H. Johnston, and J. L. Azarewicz, Proceedings of the IEEE **76**, 1510 (1988).

[12] B. Hidding, O. Karger, T. Konigstein, G. Pretzler, G. G. Manahan, P. McKenna, R. Gray, R. Wilson, S. M. Wiggins, G. H. Welsh, et al., Scientific Reports **7** 42354, (2017).

[13] A. J. Mackinnon, Y. Sentoku, P. K. Patel, D. W. Price, S. Hatchett, M. H. Key, C. Andersen, R. Snavely, and R. R. Freeman, Phys. Rev. Lett. **88**, 215006 (2002).

[14] S. C. Wilks, A. B. Langdon, T. E. Cowan, M. Roth, M. Singh, S. Hatchett, M. H. Key, D. Pennington, A. MacKinnon, and R. A. Snavely, Phys. Plasmas **8**, 542 (2001).

[15] I. Last, I. Schek, and J. Jortner, J. Chem. Phys. **107**, 6685 (1997).

[16] T. Esirkepov, M. Borghesi, S. V. Bulanov, G. Mourou, and T. Tajima, Phys. Rev. Lett. **92**, 175003 (2004).

[17] B. J. Albright, L. Yin, K. J. Bowers, B. M. Hegelich, K. A. Flippo, T. J. T. Kwan, and J. C. Fernandez, Phys. Plasmas **14**, 056706 (2007).

[18] S. Palaniyappan, B. M. Hegelich, H.-C. Wu, D. Jung, D. C. Gautier, L. Yin, B. J. Albright, R. P. Johnson, T. Shimada, S. Letzring, D. T. Offermann, J. Ren, C. Huang, R. Horlein, B. Dromey, J. C. Fernandez, and R. C. Shah, Nat. Phys. **8**, 763 (2012).

[19] S. S. Bulanov,E. Esarey,C. B. Schroeder, S. V. Bulanov, T. Zh. Esirkepov, M. Kando, F. Pegoraro, W. P. Leemans, Phys. Plasmas *23*, 056703 (2016); *ibid.* Phys. Rev. Lett. **114**, 105003 (2015).

[20] S. Steinke, A. Henig, M. Schnurer, T. Sokollik, P.V. Nickles, D. Jung, D. Kiefer, R. Horlein, J. Schreiber, T. Tajima, X.Q. Yan, M. Hegelich, J. Meyer-ter-Vehna, W. Sandnera and D. Habs, Laser and Particle Beams **28**, 215 (2010).

[21] Y. Sentoku, T. V. Liseikina, T. Zh. Esirkepov, F. Califano, N. M. Naumova, Y. Ueshima, V. A. Vshivkov, Y. Kato, K. Mima, K. Nishihara, F. Pegoraro, and S. V. Bulanov, Phys. Rev. E. **62**, 7271 (2000)

[22] A. V. Kuznetsov, T. Zh. Esirkepov, F. F. Kamenets, and S. V. Bulanov, Plasma Phys. Rep. **27**, 211 (2001).

[23] L. Willingale, S. P. D. Mangles, P. M. Nilson, R. J. Clarke, A. E. Dangor, M. C. Kaluza, S. Karsch, K. L. Lancaster, W. B. Mori, Z. Najmudin, J. Schreiber, A. G. R. Thomas, M. S. Wei, and K. Krushelnick, Phys. Rev. Lett. **96**, 245002 (2006).

[24] S. V. Bulanov and T. Zh. Esirkepov, Phys. Rev. Lett. **98**, 049503 (2007).

[25] Y. Fukuda, A. Ya. Faenov, M, Tampo, T. A. Pikuz, T. Nakamura, H. Kando, Y. Hayashi, A. Yogo, H. Sakaki, T. Kameshima, A. S. Pirozhkov, K. Ogura, M. Mori, T. Zh. Esirkepov, J. Koga, A. S. Boldarev, V. A. Gasilov, A. I. Magunov, T. Yamauchi, R. Kodama, P. R. Bolton, Y. Kato, T. Tajima, H. Daido, and S. V. Bulanov, Phys. Rev. Lett. **103**, 165002 (2009).

[26] D. Haberberger, S. Tochitsky, F. Fiuza, C. Gong, R. A. Fonseca, L. O. Silva, W. B. Mori, and C. Joshi, Nature Physics **8**, 95 (2012).

[27] Y. Sentoku, T. E. Cowan, A. Kemp, and H. Ruhl, Phys. Plasmas **10**, 2009 (2003)

[28] S. Wilks, W. Kruer, M. Tabak, and A. B. Langdon, Phys. Rev. Lett. **69**, 1383 (1992).

[29] N. M. Naumova, T. Schlegel, V. T. Tikhonchuk, C. Labaune, I. V. Sokolov, and G. Mourou, Phys. Rev. Lett. **102**, 025002 (2009).

[30] L. Willingale, P. M. Nilson, A. G. R. Thomas, S. S. Bulanov, A. Maksimchuk, W. Nazarov, T. C. Sangster, C. Stoeck, and K. Krushelnick, Phys. Plasmas **18**, 056706 (2011).

[31] F. Wagner, O. Deppert, C. Brabetz, P. Fiala, A. Kleinschmidt, P. Poth, V. A. Schanz, A. Tebartz, B. Zielbauer, M. Roth, et al., Phys. Rev. Lett. **116**, 205002 324 (2016).

[32] K. Ogura, M. Nishiuchi, A. Pirozhkov, T. Tanimoto, A. Sagisaka, T. Esirkepov, M. Kando, T. Shizuma, T. Hayakawa, H. Kiriyama, T. Shimomura, S. Kondo, S. Kanazawa, Y. Nakai, H. Sasao, F. Sasao, Y. Fukuda, H. Sakaki, M. Kanasaki, A. Yogo, S. Bulanov, P. Bolton, and K. Kondo, Opt. Lett. **37**, 2868-2870 (2012).

[33] I. J. Kim, K. H. Pae, C. M. Kim, C.-L. Lee, I. W. Choi, H. T. Kim, H. Singhal, J. H. Sung, S. K. Lee, H. W. Lee, P. V. Nickles, T. M. Jeong, and C. H. Nam, Phys. Plasmas **23**, 070701 (2016).

[34] A. Higginson, R. J. Gray, M. King, R. J. Dance, S. D. R. Williamson, N. M. H. Butler, R. Wilson, R. Capdessus, C. Armstrong, J. S. Green, et al., Nature Comm. **9**, 724 (2018).

[35] Wei M, Williams J and Arefiev A 2017 private communication at General Atomics.

[36] D. J. Stark, T. Toncian, and A. V. Arefiev, Phys. Rev. Lett. **116**, 185003 (2016);

[37] O. Jansen, T. Wang, D. J. Stark, E. d'Humières, T. Toncian, and A. V. Arefiev, Plasma Phys. Control. Fusion **60** 054006, (2018).

[38] S. S. Bulanov, V. Yu. Bychenkov, V. Chvykov, G. Kalinchenko, D.W. Litzenberg, T. Matsuoka, A. G. R.

Thomas, L. Willingale, V. Yanovsky, K. Krushelnick, and A. Maksimchuck, Phys. Plasmas *17*, 043105 (2010)

[39] S. S. Bulanov, E. Esarey, C. B. Schroeder, W. P. Leemans, S. V. Bulanov, D. Margarone, G. Korn, and T. Haberer, Phys. Rev, STAB *18*, 061302 (2015).

[40] T. D. Arber, K. Bennett, C. S. Brady, A. Lawrence-Douglas, M. G. Ramsay, N. J. Sircombe, P. Gillies, R. G. Evans, H. Schmitz, A. R. Bell, and C. P. Ridgers, Plasma Phys. Control. Fusion **57** 113001, (2015).

[41] S. Steinke, J. H. Bin, J. Park, Q. Ji, K. Nakamura, A. J. Gonsalves, S. S. Bulanov, C. Toth, J. -L. Vay, C. B. Schroeder, E. Esarey, T. Schenkel, and W. P. Leemans, in preparation.